ADVANCES IN SPANISH PHYSICAL OCEANOGRAPHY
M. Espino, J. Font, J.L. Pelegrí, A. Sánchez-Arcilla (eds.)

Scientia Marina 76S1
September 2012, 209-218, Barcelona (Spain)
ISSN: 0214-8358
doi: 10.3989/scimar.03617.19H

Fitting the last Pleistocene $\delta^{18}O$ and CO_2 time series with simple box models

ANTONIO GARCÍA-OLIVARES and CARMEN HERRERO

Departament d'Oceanografia Física, Institut de Ciències del Mar, CSIC, Passeig Marítim de la Barceloneta 37-49, 08003 Barcelona, Spain. E-mail: agolivares@icm.csic.es

SUMMARY: Based on the model of Paillard and Parrenin (2004), several box models that incorporate simple parameterizations of the oceanic CO_2 pump were developed. The models' parameters are calibrated to the $\delta^{18}O$ and CO_2 observational time series available for the last 800 kyr BP. The Paillard model performance may be improved if its CO_2 sensitivity to insolation is eliminated and different response times are assumed both for absorption/emission of CO_2 and for ablation/accumulation of ice. With these changes the correlations between simulated and experimental time series increase from 0.59 and 0.63 (for CO_2 and ice volume *V*) to 0.77 and 0.88 respectively. Oceanic CO_2 pulses of 10 to 20 kyr are found to take place at the beginning of the last nine deglaciations according to this model. The timing of the last nine terminations may also be qualitatively reproduced with a primary production model in which export depends on *V*. The dependence between CO_2 export and *V* that generates the best fit is not exponential, as expected from some evidences, but a square function. The good model-data fitting suggests that the rate of formation of deep water may be an important factor controlling the oceanic pulse that triggers the deglaciations.

Keywords: climatic changes, palaeoclimate, glacial oscillations, box models, oceanic CO_2.

RESUMEN: Ajuste de las series temporales de $\delta^{18}O$ y CO_2 del pleistoceno final con modelos simples de cajas. – Partiendo del modelo de Paillard y Parrenin (2004) se han desarrollado varios modelos que incorporan parametrizaciones simples de la bomba oceánica de CO_2. Los parámetros del modelo han sido calibrados a las series experimentales de $\delta^{18}O$ y CO_2 disponibles para los últimos 800 ka. Los resultados del modelo de Paillard pueden ser mejorados si su forzamiento insolación-CO_2 es eliminado y se suponen tiempos de respuesta diferentes para la absorción y emisión de CO_2 así como para la ablación y la acumulación de hielo. Las correlaciones entre las series simuladas y experimentales se incrementan entonces desde 0.59 a 0.63 (para CO_2 y volumen de hielo *V*) hasta 0.77 y 0.88 respectivamente. Este modelo predice pulsos oceánicos de 10 a 20 ka en el comienzo de las nueve desglaciaciones. La secuencia de desglaciaciones se puede simular cualitativamente también con un modelo de "bombeo biológico" con exportación dependiente de *V*. La dependencia entre exportación de CO_2 y *V* que genera el mejor ajuste no resultó ser exponencial como se esperaría, sino una función cuadrada. Los buenos ajustes obtenidos sugieren que la tasa de formación de agua profunda puede ser un factor importante que controla el pulso oceánico que dispara las desglaciaciones.

Palabras clave: cambios climáticos, paleoclima, oscilaciones glaciales, modelos de caja, CO_2 oceánico.

INTRODUCTION

It is considered empirically proven that changes in atmospheric CO_2 have remained tightly coupled with global climate change at least throughout the past 800000 years (Petit 1999, Pepin 2001, Siegenthaler *et al*. 2005, Lüthi 2008). However, the mechanisms responsible for pacing and moderating CO_2 changes remain to be determined. The magnitude of the marine carbon reservoir and its response to changes in atmospheric CO_2 (Broecker 1982) guarantee that the ocean plays a significant role in glacial-interglacial CO_2 change. Based on thermodynamic considerations, glacial atmospheric CO_2 would be reduced by 30 ppm simply due to the increased solubility of CO_2 in a colder glacial ocean; however this reduction would be counteracted by the reduced solubility of CO_2 in a more saline glacial ocean and by a large reduction in

the terrestrial biosphere under glacial conditions (Sigman and Boyle 2000).

The bulk of the glacial-interglacial CO_2 change therefore remains to be explained by more complex mechanisms. To date, three main types of conceptual model have been put forward (Skinner 2009): (1) those involving an increase in the export rate of organic carbon to the deep sea, either via increased nutrient availability at low latitudes or via increased efficiency of nutrient usage at high latitudes (Broecker 1982, Knox and McElroy 1984); (2) those involving a reduction in the "ventilation" of water exported to the deep Southern Ocean (Siegenthaler and Wenk 1984, Toggweiler and Sarmiento 1985); and (3) those involving changes in ocean chemistry, possibly promoted by changes in the ratio of organic carbon and carbonate fluxes to the deep sea (Archer and Maier-Reimer, 1994). In addition, "carbonate compensation" (Brovkin *et al.* 2007) would help to amplify the effect of any of the three mechanisms on the CO_2 variation (Watson and Naveira Garabato 2006). We will call the first kind of model the "export production" model and the second one the "deep water ventilation" model.

Four main mechanisms that may affect the efficiency of the deep water ventilation model have been identified: (a) changes in the surface-to-deep mixing rate efficiency (Toggweiler 1999, Gildor and Tziperman 2001, Watson and Naveira Garabato 2006) and stratification (Paillard and Parrenin 2004, Bouttes *et al*. 2010, Bouttes *et al.* 2011) in the different climatic conditions produced in glaciations; (b) extension of sea ice in the Southern Ocean producing a "capping" effect on the CO_2 release to the atmosphere (Keeling and Stephens 2001) or a retardation of the overturning rate in the Southern Ocean (SO) due to sea ice control on the residual circulation (Watson and Naveira Garabato 2006, Fischer *et al*. 2010); (c) sequestration of CO_2 in deep waters with increased standing volume during glacial climates (Skinner 2009); and (d) switch off/on of the Antarctic upwelling in the Drake Passage latitudes in cold/warm conditions (Toggweiler *et al*. 2006).

Empirical evidence of the temperature and salinity of deep water in the last glacial maximum (Adkins *et al*. 2002) suggests that very dense deep waters could have important effects on the glacial CO_2 sequestration (Paillard and Parrenin 2004). Watson and Naveira Garabato (2006) confirmed the plausibility of this idea, observing that the glacial density anomaly between Antarctic Bottom Waters (AABW) and intermediate waters was three times larger than it is today. Therefore, if the scale of the vertical mixing is inversely proportional to the density difference, the change in stratification of the deep ocean in glacial periods should be able to explain a fraction of the reduction of CO_2 input to the atmosphere due to variations in diapycnal mixing of deep waters (Watson and Naveira Garabato 2006). More recent models (Bouttes *et al*. 2010, Bouttes *et al.* 2011) have detailed the way that brine release during glacial periods could have contributed to a strong stratification. Another fraction of the CO_2 reduction could be explained by the "standing volume effect" suggested by Skinner (2009). Northern and southern water in the modern ocean mixes together in the interior to form the water mass known as Circumpolar Deep Water (CDW). A significant portion of the global ocean below one kilometre is filled from the SO by Lower Circumpolar Deep Water (LCDW), which is exported northwards into the various ocean basins from the eastward circulating Antarctic Circumpolar Current (ACC) (Sloyan and Rintoul 2001, Skinner 2009). Southern-sourced deep water was found in the deep North Atlantic down to a water depth of 2.5 km during the last glacial age (Curry and Oppo, 2005). This deep-water remained relatively poorly equilibrated with the atmosphere and is inefficiently stripped of its nutrients, thus maintaining an elevated nutrient and dissolved inorganic carbon content. This evidence suggests that a fraction of the CO_2 change was probably produced by the increase in southern-sourced water, which is richer in CO_2.

Finally, according to Toggweiler *et al.* (2006), any process producing a (global or southern) tropospheric warming would imply poleward-shifted westerlies. This would produce stronger wind-stress at the latitude of the Drake Passage and stronger upwelling of deep water in SO. However, it is not obvious that the overturning rate of the ocean must have been significantly different between modern and glacial periods (Wunsch 2003), and empirical evidences and comparisons of coupled general circulation models for glacial conditions suggest there was very little change in the strength of the zonal wind stress on the SO and no clear shift in the location of the westerlies belt (Fischer *et al*. 2010).

A simple box model that takes into account the changes in the overturning rate and biological exportation of CO_2 was proposed by Pelegrí (2008) to explain the CO_2 glacial-interglacial cycles. This model suggested that during the transition from glacial to interglacial the supply of inorganic nutrients and carbon to the upper ocean could initially increase through enhanced remineralization of the pool of dissolved organic carbon followed by greater supply from the deep ocean. The results reproduce well the sawtooth-like oscillations observed during the last four glacial cycles but this study did not aim to explain the physical triggers of these changes in nutrient and carbon supply. Ganopolski *et al.* (2010) showed that Earth climate models of intermediate complexity, such as CLIMBER-2, are able to reproduce the major aspects of glacial cycles under orbital and greenhouse forcing quite realistically. However, the CO_2 forcing has to be introduced independently of the orbital forcing.

The effect of deep stratification on CO_2 sequestration has been included in a box-model of Pleistocene climatic oscillations by Paillard and Parrenin (2004). In spite of its simplicity, this model is the first one to accurately simulate the timing of all the glacial termi-

nations as well as the whole set of maxima and minima of the $\delta^{18}O$ oscillations observed in the past 3.5 million years. This may be a sign of the crucial role played by the stratification and Southern Ocean CO_2 pulse in the onset of deglaciations.

Here, the Paillard and Parrenin (2004) model has been generalized and calibrated to the $\delta^{18}O$ and CO_2 time series available for the last 800 ky (Petit *et al.* 1999, Monnin *et al.* 2001, Pepin *et al.* 2001, Lisiecky and Raymo 2005, Siegenthaler *et al.* 2005, Lüthi *et al.* 2008). The objective is: (i) to obtain the set of parameters that best fit the late Pleistocene time series in Paillard's original model; (ii) to investigate several generalizations of Paillard's model by introducing some simple submodels for the export production, the strength of deep stratification and other mechanisms; and (iii) to analyse how the different submodels affect the data fit.

The next section describes the structure of the initial Paillard and Parrenin (2004) model and its best calibrations to the $\delta^{18}O$ and CO_2 data for the last 800 kyr. A biological export rate is next introduced instead of the original mechanism and the model obtained is calibrated and analysed. Also, an alternative model with two different response times for the CO_2 emission and absorption is analysed. This is followed by a study of the model that results when two different response times are introduced for accumulation and ablation of ice. Next, we describe the patterns found when the different model calibrations are compared. Finally, the results and conclusions are summarized.

THE MODEL

The structure of the original Paillard and Parrenin (2004) model is the following:

$$dV/dt = (V_r - V)/\tau_V \quad \text{with} \quad Vr = -xC - yI_{65} + z$$
$$dA/dt = (V - A)/\tau_A$$
$$dC/dt = (C_r - C)/\tau_C \quad \text{with} \quad Cr = \alpha I_{65} - \beta V + \gamma O(F) + \delta$$

where V and A are dimensionless indexes for non-Antarctic ice volume and extent of Antarctic ice sheet respectively, C is a dimensionless index for atmospheric CO_2, I_{65} is the daily insolation at 65°N on 21 June, $O(F)$ is the deep ocean contribution to the CO_2 of reference, which in the original model is $O(F)=H(-F)$, where H is the Heaviside function ($H=1$ if $F<0$; $H=0$ otherwise), and F is the salty-bottom water-formation-efficiency parameter $F=aV-bA-cI_{60}+d$. F increases with ice volume V and decreases when continental shelf areas are reduced (through A) and when I_{60} (daily insolation at 60°S on 21 February) increases.

The main variables V, A and C tend to decay exponentially to a reference state V_r, V and C_r in characteristic times τ_V, τ_A and τ_C, respectively. Reference volume (V_r) decreases when C increases, and when I_{65} is high. The CO_2 of reference (C_r) increases when I_{65} is high through parameter α and when the oceanic pulse of CO_2 is on (through parameter γ), and decreases when the ice volume increases. The β parameter represents the feedback between ice volume V and CO_2.

In this study, daily insolations of the last 800 ky are obtained from the Berger (1978) and Berger and Loutre (1991) software. Insolations have been normalized with their standard deviations to obtain I_{65} and I_{60}. No lower bound is imposed on the V, C and A variables, which may take positive or negative values because they represent relative and not absolute variations.

In Paillard and Parrenin (2004) no precise tuning of the parameters was performed but a table with central value and range for the parameters was presented. We could not reproduce the results displayed in that work except if τ_V is increased from 15 to 18 kyr (Table 1). Two different integration methods were used for the differential equations (Mathematica-7.0 internal algorithms with four digits precision and Predictor-Corrector explicit method with time step of 25 years) and the results were coincident. Given the strong nonlinearity in the variable C dynamics, at least 32000 steps are needed in the latter algorithm to grant that results are independent of the number of steps.

A systematic search of the set of parameters that lead to maximum correlation was implemented around this central case. Correlations of the V and C time series with the (respectively) $\delta^{18}O$ and CO_2 experimental series available for the last 800 kyr were calculated. The expression for the statistical correlation is the following:

$$Cor[s_1, s_2] = \frac{(s_1 - E[s_1]) \cdot (s_2 - E[s_2])}{(N-1)\sigma[s_1]\sigma[s_2]}$$

where $Cor[s_1,s_2]$ is the correlation between the time series s_1 and s_2 , $E[x]$ is the expected value (mean) of x, the dot symbol denotes scalar product, $\sigma[x]$ is the standard deviation of x, and N is the number of components of arrays s_1 and s_2.

The correlations obtained are shown in columns 3 and 4 of Table 1. As can be observed in column 3 of the table, the correlations of the central case of Paillard and Parrenin (2004) can be improved from 0.59 and 0.63 to 0.62 and 0.64 for CO_2 and ice volume, respectively, when the α parameter is maintained at 0.15 (hereafter model *P*). However, best correlations are obtained when this parameter takes the zero value (column 3, model *PB*): 0.67 and 0.71. This parameter represents a direct forcing of I_{65} on atmospheric CO_2 and its physical interpretation is not clear, given that the CO_2 response to ice volume is already included in the model. Thus, we have eliminated this parameter from the model hereafter. The second and third panels of Figures 1 and 2 show the ice volume and CO_2 time series simulated with these two parameter sets. The main difference between the two cases appears in the CO_2 time series, where the oscillations of 41 and 21 kyr in the case with $\alpha=0$ present a lower amplitude than in the case with $\alpha=0.15$.

TABLE 1. – Central values of the models studied. Columns 2 to 8 correspond to: (2) Paillard (2004) model with τ_V=18 kyr; (3) best fit of previous model with α=0.15 (model *P*); (4) best fit of previous model (model *PB*); (5) model with export production (model *EP*); (6) model with two relaxation times for C (model 2τ); (7) previous model with oceanic pulse exponentially dependent on stratification (model *Ex*); (8) model with two relaxation times for *V* (model 4τ). The last four lines respectively correspond to correlation for CO_2, correlation for *V*, standard deviation of error time series for *C*, and standard deviation of error time series for *V*.

Parameter	Paillard τ_v=18 kyr	Paillard Best α=0.15 *P*	Paillard Best *PB*	Export Prod. *EP*	τ_C, τ_{C2} 2τ	Exp Pulse *Ex*	τ_C, τ_{C2}, τ_V, τ_{V2} 4τ
α	0.15	0.15	0	-	-	-	-
β	0.5	0.345	0.496	0.76	0.496	0.48	0.496
γ	0.5	0.51	0.506	0.49	0.513	0.44	0.45
δ	0.4	0.3	0.4	0.4	0.434	0.45	0.43
ε	-	-	-	0.8	-	-	-
k	-	-	-	0.47	-	-	-
V_m	-	-	-	0.5	-	-	-
x	1.3	1.46	1.32	0.85	1.29	1.73	1.35
y	0.5	0.45	0.45	1	0.5	0.2	0.3
z	0.8	0.85	0.8	0.92	0.85	0.966	0.92
a	0.3	0.3	0.3	-	0.3	0.3	0.3
b	0.7	0.66	0.71	-	0.71	0.71	0.71
c	0.01	0.005	0.005	-	0.005	0.01	0.005
d	0.27	0.27	0.27	-	0.27	0.255	0.26
τ_c	5000	5500	5000	100	800	2907	1100
τ_{c2}	-	-	-	6500	4500	6667	6500
τ_v	18000	22000	15000	3667	12000	750	9500
τ_{v2}	-	-	-	500	-	-	6283
τ_A	12000	10250	10500	-	11333	11200	11500
λ	-	-	-	-	-	38	-
Corr C	0.59	0.60	0.67	0.45	0.75	0.77	0.77
Corr V	0.63	0.65	0.71	0.58	0.82	0.84	0.88
σErr $_C$		0.88	0.81	1.05	0.73	0.678	0.677
σErr $_V$		0.84	0.77	0.91	0.61	0.55	0.48

EXPORT PRODUCTION MODEL

Martínez-Garcia *et al.* (2009) observed that the export productivity in the subantarctic Atlantic during glacial stages grew exponentially. This suggests that the export production in the SO could be driven by changes in the supply of iron by dust, which is known to be exponentially correlated with global ice volume. We tested the extent to which an export-like mechanism that is exponentially dependent on ice volume *V*, instead of the original physical mechanism is able to generate fits of similar correlation to the ones obtained with the original model (labelled *P*). With this purpose, the third term in the r.h.s. of the expression for C_r is replaced by an expression that represents the biological rate of exportation of the SO (*B*), in the following way:

$$B = \varepsilon(e^{kV} - 1) \text{ if } V>0 \text{ and } B=0 \text{ elsewhere}$$

However, with this choice the *V* dynamics is unstable and *V* increases indefinitely for most of the ε values. This derives from the positive feedback between *V* and *C* exportation. To avoid this, we assume then that *B*(*V*) has a bell-shaped form that increases with *V* until a V_m value and then decreases to zero for very high *V* values. This is equivalent to assuming that extremely large ice volume would produce a negative effect on the biological activity, possibly because of very low temperatures in the SO. The new expression is the following:

$$\delta + B = \delta \{- \varepsilon \exp [- (0.5(V - V_m)/\sigma)^2]\}$$
$$\text{where: } \sigma = k\{1 - \text{Tanh } [2(V - V_m)]\}$$

In this expression we have joined the *b* and δ terms in the expression for C_r and we have assumed that σ decays quickly with *V* after a certain value V_m.

The best fit obtained with this model (labelled *EP*) produces the time series shown in the first panel of Figures 1 and 2. The correlations are 0.45 and 0.58 for *C* and *V* respectively, which are worse than the ones obtained for the other models analysed. The set of parameter values used is shown in Table 1, column 5. For these values, the function δ+B that represents the exportation-like contribution to the reference carbon C_r, is roughly square-shaped (see Fig. 3), with a maximum for *V* values that correspond roughly to interglacials and the first third of glacial periods, a quick decrease to a minimum value for *V* values corresponding to the remaining glacial period, and an increase to the maximum value afterwards. The decrease is instantaneous instead of exponential but no better fit was found for a gradual exponential decrease of the function.

As can be seen in Figure 1, the ice volume is poorly simulated but, even so, many of the ice ages can be identified. The model is able to reproduce qualitatively the nine terminations. However, the terminations VI and V are poorly simulated because the CO_2 interglacial pulse is widely underestimated.

The correlation of *C* with the inorganic carbon data is lower than the correlation of *V* with the corresponding data, even though a visual inspection could sug-

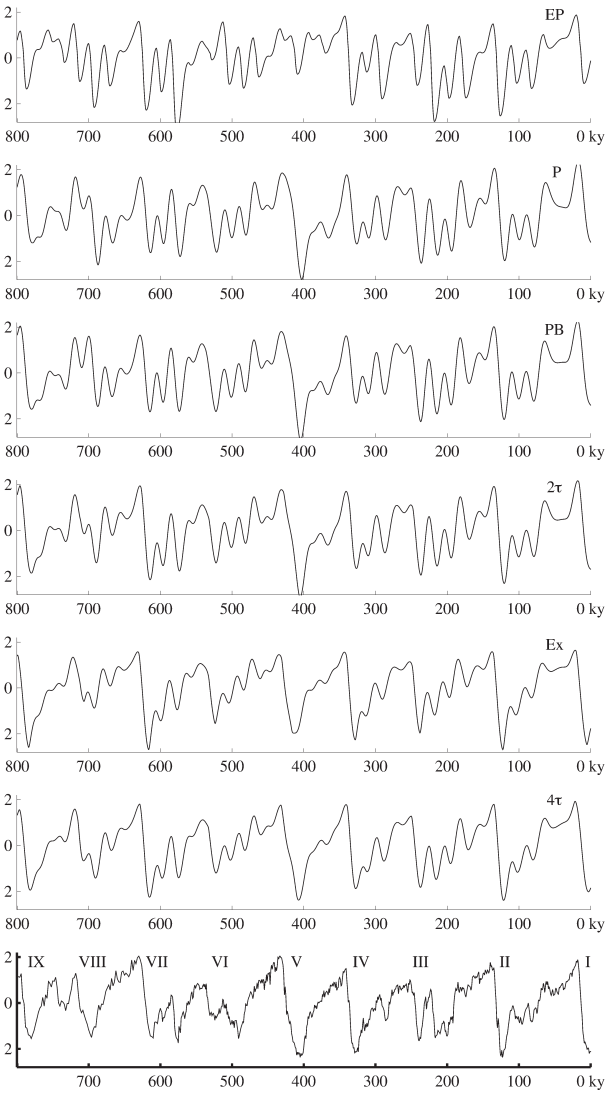

FIG. 1. – Best fits obtained for the $\delta^{18}O$ observed time series, when (top to bottom) the following models are used: (a) Paillard model without deep stratification mechanism and with a model for biological exportation; (b) original Paillard model; (c) original Paillard model without astronomical forcing on CO_2; (d) Different response times for emission and absorption of CO_2; (e) previous model with oceanic pulse of CO_2 exponentially dependent on the stratification; and (f) model with different response times for emission and absorption of CO_2 as well as for accumulation and ablation of ice. The simulations are compared with the experimental time series (bottom panel) available for ice volume (Lisiecki, 2005).

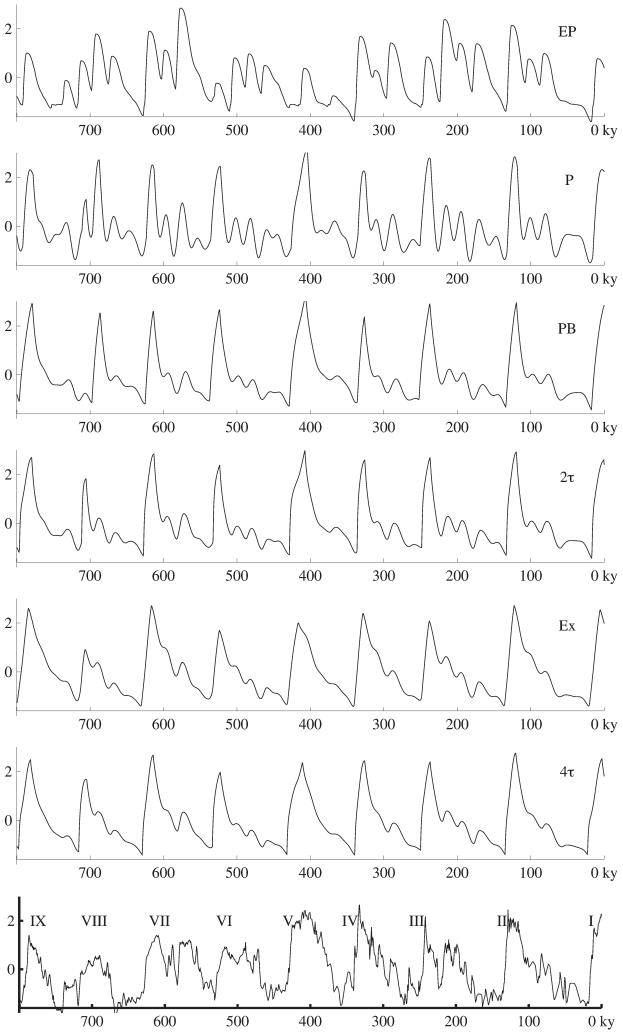

FIG. 2. – Best fits obtained for the CO_2 observed time series, when (top to bottom) the following models are used: (a) Paillard model without deep stratification mechanism and with a model for biological exportation; (b) original Paillard model; (c) original Paillard model without astronomical forcing on CO_2; (d) Different response times for emission and absorption of CO_2; (e) previous model with oceanic pulse of CO_2 exponentially dependent on the stratification; and (f) model with different response times for emission and absorption of CO_2 as well as for accumulation and ablation of ice. The simulations are compared with the experimental time series (bottom figure) available for CO_2 (Lüthi *et al*. 2008). Roman numbers corresponding to the nine glacial terminations have been superimposed.

gest that the *C* fit is better than the *V* fit. This probably derives from our tendency to give more importance to coincidence of peaks than to coincidence of other parts of the curve. In this regard, the peaks in *V* are less apparent than those in *C,* and are mixed with many secondary peaks.

TWO RESPONSE TIMES FOR *C*

Given that the deep stratification mechanism, as introduced by Paillard and Parrenin (2004), generates a fit to the data that is better than model *EP*, we tried to introduce changes in the *P* model that could improve the correlations obtained in columns 2 and 3 of Table 1. Observation of panels 2 and 3 of Figure 2 suggests that the correlation between the *C* time series and the experimental data could increase if the *C* plot was closer to a triangular sawtooth shape, in particular during glaciations. This shape could possibly be obtained if the response time for the CO_2 absorption was longer than the response time for the CO_2 emission. Thus, we used a different relaxation time (τ_{C2}) for the periods where $C>C_r$. The calibration of this model (labelled 2τ hereafter) with this additional parameter (column 6 of Table 1) generates a best fit with

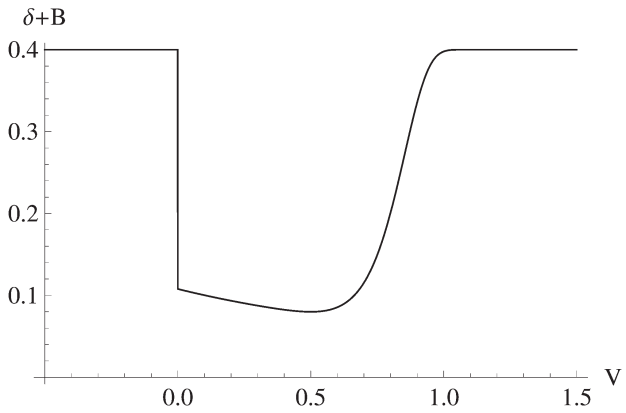

FIG. 3. – Function δ+B(*V*) used by the export production model (*EP*) in the best fit case.

correlations of 0.74 and 0.82 for *C* and *V* respectively, which is better than the one obtained with model *PB* (0.67 and 0.71 respectively). As was observed in Figure 1 (4th panel), in this case the *V* minima obtained at the terminations are deeper than in the previous case (3rd plot) and this produces a graph that is closer to the experimental time series.

OCEANIC PULSE EXPONENTIALLY DEPENDENT ON STRATIFICATION

Model *P* generates oceanic CO_2 pulses *O*(*F*) with a strong non-linear dependence on the stratification parameter *F*, through the Heaviside function:

O(*F*)= *H*(–*F*). Thus, during the glacial periods the contribution of this term is zero. An alternative way to generate sawtooth like oscillations in the glacial periods could be to allow for some non-zero CO_2 emission when *F* is positive but small. With this purpose, the oceanic pulse (third term in the r.h.s. of C_r expression) was modelled in the following way:

$$O(F)= \gamma e^{-\lambda F} \text{ if } F>0 \text{ and } O(F)=\gamma \text{ elsewhere.}$$

If *O*(*F*) is constrained to be 0.2γ when *F*=0.05 then λ is approximately 32.

The time series corresponding to the best fit obtained for this model (which will be labelled *Ex*) is shown in panel 5 of Figures 1 and 2, and the set of parameters used are displayed in column 7 of Table 1.

The correlations for *V* and *C* in this case increase to 0.84 and 0.77, respectively. The carbon time series is closer to a sawtooth oscillation than in the previous models. The relatively high damping of the high frequency oscillations (21 and 42 kyr) in the *V* series derives from the *y* parameter, or sensitivity to the I_{65} insolation, which takes a small value (0.2). Model *Ex* is the one in which the sawtooth-like oscillation is most clearly dominant over the 41 and 21 kyr cycles and, in this aspect, is the one that best resembles the experimental time series.

TWO RESPONSE TIMES FOR *V*

By introducing two different response times for accumulation and ablation of ice in model 2τ (τ_{V1} for periods when $V<V_r$ and τ_{V2} when $V>V_r$), a new model is obtained and is labelled 4τ hereafter. The best fit of model 4τ has the same correlation for *C* as model *Ex* (0.77) but its correlation for *V* is better (0.88) (last column of Table 1). Panel 6 of Figures 1 and 2 shows the simulated *V* and *C* time series. The effect of the *y* parameter (sensitivity to the I_{65} insolation) on the ice volume time-series simulated can be observed again. In this case, the *y* value is 0.3, which is between the 0.2 value of model *Ex* and the 0.5 value of model 2τ. The *C* series has a saw-shaped form as in model *Ex*, and the 42-kyr oscillations are similarly damped due to the large value of τ_{C2} in both cases (6667 and 6500 yr, respectively). This contrasts with model 2τ, where high frequency oscillations in *C* are more apparent. This is because τ_C and τ_{C2} are both smaller (4500 and 800 respectively) in this model.

The 21 and 42-kyr oscillations in the *V* time series are also slightly more damped than in model 2τ due to the influence of *C* on *V*. The *V* time series resembles a sawtooth oscillation, as in the experimental data, even though the maximum at 515 kyr is overestimated. The minima at 700 and 575 kyr are deeper in this simulation than in model *Ex* and more similar to the experimental data, and the maximum at 220 kyr is suitably simulated by this model. The shape of the cycles I, III, IV and VII are also suitably simulated.

COMPARISON OF THE SIX FITS

The analysis of Table 1 gives some hints to the conditions that lead to the best data fits.

The *a* parameter (sensitivity of *F* to *V*) is 0.3 for all the models. The *b* parameter is always between 0.66 and 0.71, the *c* parameter is always small: 0.005 to 0.01 and the *d* parameter, which controls the magnitude of *F*, is between 0.255 and 0.27. These four parameters have to be in a narrow range to allow the model to work properly, because they control the *F* value, which connects/disconnects the oceanic pulse that drives the deglaciations.

The addition γ+δ is between 0.81 and 0.96 and τ_A is between 10250 and 12000 in all the models.

Model *EP* requires a very high value (0.76) for the β parameter (sensitivity of C_r to *V*) and a very high value (1) for the *y* parameter (sensitivity of *V* to I_{65}) to work properly. It also uses the smallest value (100 yrs) for the τ_C parameter (quick response of *C* to the variation of C_r). In the remaining models the value of the β parameter is in the range 0.345 to 0.50.

Model *Ex* has the highest value (1.73) for the *x* parameter (sensitivity of *V* to *C*) and the lowest value (0.2) for the *y* parameter (sensitivity of *V* to I_{65}), which explains the relatively lower presence of high-frequency oscillations in *V*(*t*) and *C*(*t*). The parameter *y* has

to take values between 0.2 and 0.3 to produce a low amplification of the 21- and 42-kyr cycles and thus, a "roughness" in the *V* series similar to the one observed in the experimental data.

τ_{C2} is between 2.3 and 5.9 times τ_C for the two best models (*Ex* and 4τ), which implies that these models need longer times for absorption than for emission of CO_2. τ_V is larger than τ_{V2} in models *EP* and 4τ, which implies that these models need longer times for accumulation than for ablation of ice.

As can be observed in Figure 1, all models have problems in accurately simulating the minimum of *V* at 200 kyr (cycle II), the timing of the *V* minimum at 490 kyr (Termination VI) and the maximum ice volume at 750 kyr BP (except, to some extent, model *EP*). In addition, the minimum ice volume just after 500 BP is not simulated on time by any model except, poorly, by model *EP* and by model *P*.

It may be observed that all models have problems in simulating the glacial cycle between 600 and 500 kyr, especially the timing of its termination. Model 4τ predicts the termination VII too early but it is the only one to accurately predict the timing of Terminations II and IV. Inaccurate fitting of the timing of terminations probably derives from limitations of both model and $\delta^{18}O$ records. A common way of estimating time in paleoclimate records is to stretch, squeeze and shift a record's chronology in order to align it with a template indicative of changes in the Earth's orbital and rotational configuration, a process generally referred to as orbital tuning (Huybers 2010). For this reason, it is not clear that the time scale of the data is better or worse than the time scale of the model (within, let's say, a quarter period of the fastest forcing, the precession, i.e. ±6 kyr). This is particularly true for the timing of terminations, which apparently are not linearly correlated with the astronomical forcing intensity (see e.g. Parrenin and Paillard 2003). For this reason, a "better fit" of the timing of terminations of the $\delta^{18}O$ data may not be an improvement, because the data are not necessarily very accurate in their estimation of the precise dates when terminations take place.

Time series for the fit error were obtained by subtracting the simulated and experimental time series resulting from dividing every time series by its standard deviation. The last four lines in Table 1 correspond to correlations obtained for the carbon variable *C*, correlation for *V*, standard deviation of the time series for the error in the CO_2 prediction, and standard deviation of the time series for the error in the ice volume prediction, respectively. As expected (Table 1), the standard deviation of the errors decreases in parallel with the increase in correlation. The maximum gain of correlation between one model and the following one occurs when we use two different parameters for the emission and absorption of CO_2 (column 6).

Figure 4 compares the different contributions to C_r in the original model of Paillard and Parrenin (2004), model *P*, model *Ex*, and model 4τ. In the first two models (panels 1 and 2) the contributions are oceanic CO_2 pulses (thick line), feedback V-CO_2 (thin line) and I_{65} forcing (dashed line). In the third and fourth panels, no astronomical forcing on *C* appears because it is not used by the models, and an additional inertia term (or transitory separation of the *C* and C_r variables) has been included (this inertial contribution has not been displayed in panels 1 and 2 to avoid excessively complicated figures). The addition of all these contributions generates the corresponding time series displayed in Figure 1. Thick lines (step-like) in the plots show the intensity of the oceanic CO_2 pulses, which are different from zero always in coincidence with the start of deglaciations. The second model (*P*) gets a finer fit to data by producing several short oceanic CO_2 pulses in the period between 725 and 500 kyr BP. In order to generate appropriate fits, the third and fourth models have to compensate for the lack of astronomical forcing on the CO_2 pumping with an enhanced V-CO_2 feedback, which is produced by larger values of the product βV.

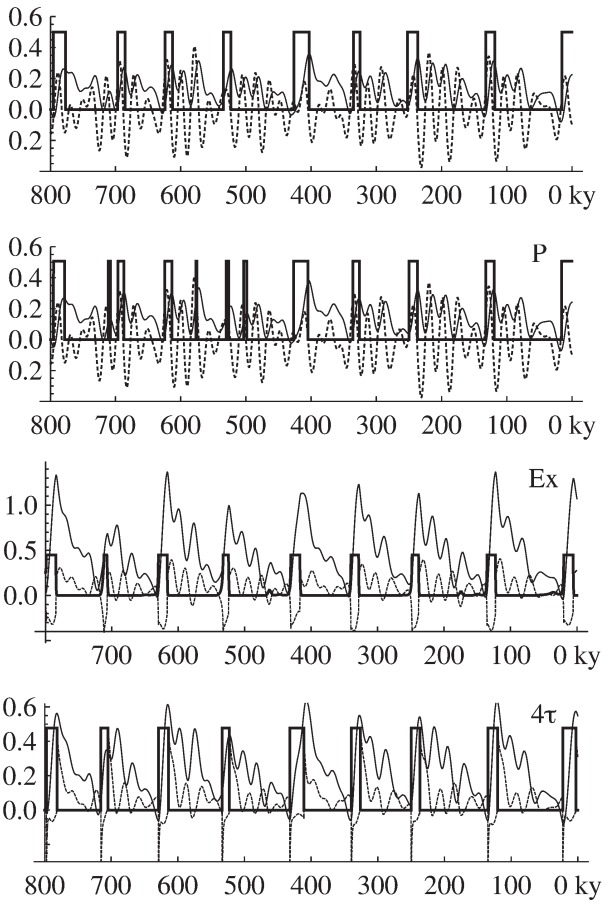

FIG. 4. – Contributions to C_r used by (top to bottom): the original Paillard (2004) model, the best tuned Paillard's model with α=0.15 (model *P*), the model with oceanic pulse as a exponential function of stratification (model *Ex*), and the model with four response times (model 4τ). In the first two models (panels 1 and 2) the contributions are oceanic CO_2 pulses (thick line), feedback V-CO_2 (thin line) and I_{65} forcing (dashed line). In the third and fourth panels, the astronomical forcing is zero and the inertia term (or transitory separation of the *C* and C_r variables) has been included (dotted line).

In model *Ex* the oceanic pumping consists of a set of rectangular pulses that are followed by an exponential decay. However, the exponential tails are so short that the pulses are almost rectangular, as in all other cases. This illustrates the strong non-linearity of the oceanic pulse response to changes of the deep water generation efficiency F in all the models studied. As can be observed in the second panel, short and isolated oceanic pulses (such as that at 580 kyr) are not able to trigger deglaciations. However, two short but very close pulses could be able to trigger them (pulses around 700 kyr in panel 2). In model 4τ (panel 4), the deglaciations start following oceanic pulses with a duration of between 11 kyr (terminations VIII and VI) and about 20 kyr (terminations V and I).

FINAL DISCUSSION

Starting from the Paillard and Parrenin (2004) model, several box models incorporating simple parameterizations of the oceanic CO_2 pumping and response times of carbon and ice volume were developed. The models' parameters were calibrated to provide the best fit to the $\delta^{18}O$ and CO_2 experimental time series available for the last 800 kyr BP. The Paillard and Parrenin (2004) model is insensitive to the α parameter (direct forcing between I_{65} insolation and CO_2) and the Sun's effect seems to emerge only through the filter of global ice volume. The fit of this model to observational data may be improved if different response times are assumed both for absorption/emission of CO_2 and for ablation/accumulation of ice. Correlations between simulated and experimental time series increase from 0.59 and 0.63 to 0.77 and 0.88 for CO_2 and V, respectively. This means that 59% and 77% of the variance is explained respectively by the best fit.

Several modifications of the Paillard and Parrenin (2004) model that lead to the right timing of the last nine terminations were tested. In particular, the qualitative behaviour of the last eight glacial-interglacial cycles may be roughly reproduced with an export production model with export dependent on ice volume. However, in this model, the best fit corresponded to a dependence between CO_2 export and V that was not exponential as proposed by (Martínez-García *et al*. 2009) but a square function. In our formulation, biological export alone was not able to simulate the experimental data as accurately as the other models, even though some kind of biological export of CO_2 is very probably acting in synergy with physical processes in the glacial-interglacial dynamics.

Two models (*Ex* and 4τ) show a good performance in the simulation of the ice volume observed in the last eight glacial-interglacial cycles and even in many details of that signal belonging to the scale from 21 to 42 kyr. The good fits obtained in both cases suggest that density of deep water and its rate of formation may be an important factor controlling the oceanic pulse that triggers the deglaciations. Schmittner (2007) has confirmed, with a global climate model, the sensitivity of atmospheric CO_2 to processes that affect stratification in SO waters. In our analysis, oceanic pulses that strongly depend, in a non-linear way, on the deep ocean stratification are necessary to trigger deglaciations. The pulses obtained in the best models are always very close to the Heaviside function proposed by the original work of Paillard and Parrenin (2004). Oceanic CO_2 pulses with a duration of between 10 and 20 kyr were found at the beginning of the nine last deglaciations according to the best model analysed (4τ). In addition, different response times for emission and absorption of CO_2 and for accumulation and ablation of ice are necessary to obtain the best fit to the available data. Accumulation and ablation of ice are different physical mechanisms that could have different characteristic times. However, the two response times for emission and absorption of CO_2 are more difficult to explain. To decide whether these two response times correspond to real physical mechanisms, a deeper understanding of the long-term transfer rates in the carbon cycle should be achieved.

Björkström (1979) identified the two slowest response times for the emission of CO_2 to the atmosphere to be: (i) that of the organic carbon of dead material in soils and (ii) travel time of the CO_2 from the deep ocean compartments to the surface. These authors used 1000 yr as an order of magnitude for both parameters. Brovkin *et al*. (2002) used the range 400-1000 yr to model the slow soil response with the CLIMBER-2 paleoclimatic model. The characteristic time of CO_2 absorption in the long-term scales is related to the CO_2 advection from the surface into the deep ocean according to Björkström (1979) and it should be, again, of the order of 1000 yr.

Our result $\tau_{C2}>\tau_{C1}$ could be meaningful if the characteristic time of deep water circulation was longer than the long-term emission time of soils. Montenegro *et al.* (2007) found that 25% of an instantaneous CO_2 release to the atmosphere remains there after 5000 years. Archer *et al.* (2009) reviewed the literature on the carbon cycle, which agrees that 20% to 35% of an instantaneous CO_2 release remains in the atmosphere in 200 to 2000 yr, after equilibration with oceans. Due to oceanic acidification, subsequent dissolution of $CaCO_3$ increases the uptake capacity of oceans in the scale of 3 to 7 kyr. These results are apparently coherent with the order of magnitude of the τ_{C2} parameter that we have found. However, more investigation is needed to have a precise understanding of the long-term carbon cycle.

A different problem is deciding what confidence we can give to those models with higher correlations, given that the record used for the past ice volume probably suffers different biases. Indeed, the record is a stack of $\delta^{18}O$ data from benthic foraminifera, and the ratio $^{18}O/^{16}O$ is known to depend on both the isotopic composition and the temperature of the water where the foraminifera develops. Siddall *et al*. (2009) found that ice volume becomes increasingly sensitive to tem-

perature change at low temperatures. Waelbroeck *et al.* (2002) found that the relationship between $\delta^{18}O$ and ice volume is not linear, since $\delta^{18}O$ decreased faster than the increase in ice volume at the beginning of the last glaciations, and then progressively more slowly until the ice sheets reached their maximum size. This may produce uncertainties greater than 20% for the ice volume estimations in some periods. Therefore, the models with the largest correlations between predicted ice volume and $\delta^{18}O$ are not necessarily better than other models with slightly lower correlation because of the uncertainty in the observational data. This is a complex and important question requiring an additional mathematical analysis that we leave for a future work. Fortunately, there is no such problem for CO_2, which is directly measured in ice cores.

It may be argued that it is not surprising to get good fits (Fig. 1) using models with many parameters. This is particularly true when experimental data are fitted to generic mathematical functions that are dependent on an arbitrary number of parameters. However, it is not so easy to get the same good fit with mathematical expressions that imitate geophysical mechanisms such as feedbacks and pumping rates. An additional outcome from mechanistic box models of this kind is that they point to specific physical mechanisms that are potentially drivers of the observed changes. Thus, when good fits are obtained with such models, the specific physical mechanisms modelled should be investigated in more detail to confirm them (and not an alternative mechanism producing a similar behaviour) as inducers of the observed dynamics.

ACKNOWLEDGEMENTS

This is a contribution to projects MOC-2 (ref. no. CTM2009-06438-C02-01) and TIC-MOC (ref. no. CTM2011-28867) funded by the Spanish R+D Plan 2008-2011. We thank Didier Paillard for useful comments on the manuscript. We also thank Carles Pelejero and Eva Calvo for interesting suggestions and help with the experimental data, Jose Luis Pelegrí for his exhaustive revision and Roger Olivella for his help with the Berger and Loutre software.

REFERENCES

Adkins J.F., McIntyre K., Schrag D.P. 2002. The salinity, temperature and $\delta^{18}O$ of glacial deep ocean. *Science* 298: 1769-1773.

Archer D., Maier-Reimer E. 1994. Effect of deep-sea sedimentary calcite preservation on atmospheric CO_2 concentration. *Nature* 367: 260-263.

Archer D., Eby M., Brovkin V., Ridgwell A., Cao L., Mikolajewicz U., Caldeira K., Matsumoto K., Munhoven G., Montenegro A., Tokos K. 2009. Atmospheric Lifetime of Fossil Fuel Carbon Dioxide. *Annu. Rev. Earth Pl. Sc*. 37: 117-133.

Bard E. 1988. Correction of accelerator mass spectrometry ^{14}C ages measured in planktonic foraminifera: Paleoceanographic implications. *Paleoceanography* 3: 635-645.

Berger A. 1978. A simple algorithm to compute long term variations of daily or monthly insolation. *Contr. 18*. Inst of Astronomy and Geophysics . Université Catholique de Louvain. Louvain-la-Neuve. Belgium.

Berger A., Loutre M.F. 1991. Insolation values for the climate of the last 10 million years. *Quaternary Sci. Rev*. 10: 297-317.

Björkström A. 1979. A Model of CO_2 Interactions between Atmosphere, Oceans, and Land Biota. In: Bolin, B., Degen E.T., Kempe S., Ketner P. (eds.), *The Global Carbon Cycle. Scientific Committee on Problems of the Environment (SCOPE)*, Chap. 15. Available at: www.icsu-scope.org/downloadpubs/scope13/contents.html

Brovkin V., Bendtsen J., Claussen M., Ganopolski A., Kubatzki C., Petoukhov V., Andreev A. 2002. Carbon cycle, Vegetation and Climate Dynamics in the Holocene: Experiments with the CLIMBER-2 Model. *Global Biogeochem. Cy.* 16(4): 1139.

Brovkin V., Ganopolski A., Archer D., Rahmstorf S. 2007. Lowering of glacial atmospheric CO_2 in response to changes in oceanic circulation and marine biogeochemistry. *Paleoceanography* 22: PA4202.

Bouttes N., Paillard D., Roche D.M. 2010. Impact of brine-induced stratification on the glacial carbon cycle. *Clim. Past Discuss*. 6: 681-710.

Bouttes N., Paillard D., Roche D. M., Brovkin V., Bopp L. 2011. Last Glacial Maximum CO_2 and $\delta^{13}C$ successfully reconciled. *Geophys. Res. Lett.* 38: L02705.

Broecker W.S. 1982. Glacial to interglacial changes in ocean chemistry. *Prog. Oceanogr.* 11: 151-197.

Curry W.B., Oppo D.W. 2005. Glacial water mass geometry and the distribution of $\delta^{13}C$ of ΣCO_2 in the western Atlantic Ocean. *Paleoceanography* 20: PA1017.

Fischer H., Schmitt J., Lüthi D., Stocker T.F., Tschumi T., Parekh P., Joos F., Köhler P., Völker C., Gersonde R., Barbante C., Le Floch M., Raynaud D., Wolff E. 2010. The role of Southern Ocean processes in orbital and millennial CO_2 variations – A synthesis. *Quaernary. Sci. Rev*. 29: 193-205.

Gildor H., Tziperman E. 2001. Physical mechanisms behind biogeochemical glacial-interglacial CO_2 variations. *Geophys. Res. Lett*. 28: 2421-2424.

Huybers P. 2010. Combined obliquity and precession pacing of the late Pleistocene glacial cycles. *Geophys. Res. Abstracts* 12: EGU2010-15001, EGU General Assembly 2010. Available at: www.people.fas.harvard.edu/~phuybers/Doc/total_draft.pdf

Keeling R.F., Stephens B.B. 2001. Antarctic sea ice and the control of Pleistocene climate instability. *Paleoceanography* 16: 112-131.

Knox F., McElroy M. 1984. Changes in atmospheric CO_2: Influence of marine biota at high latitude. *J. Geophys. Res*. 89: 4629-4637.

Lisiecki L. E., Raymo M. E. 2005. A Pliocene-Pleistocene stack of 57 globally distributed benthic $\delta^{18}O$ records. *Paleoceanography* 20: PA1003.

Lüthi D., Le Floch M., Bereiter B., Blunier T., Barnola J.-M., Siegenthaler U., Raynaud D., Jouzel J., Fischer H., Kawamura K., Stocker T.F. 2008. High-resolution carbon dioxide concentration record 650,000-800,000 years before present. *Nature* 453: 379-382.

Martínez-Garcia A., Rosell-Melé A., Geibert W., Gersonde R., Masqué P., Gaspari V., Barbante C. 2009. Links between iron supply, marine productivity, sea surface temperature, and CO2 over the last 1.1 Ma. *Paleoceanography* 24: PA1207.

Monnin E., Indermühle A., Dällenbach A., Flückiger J., Stauffer B., Stocker T.F., Raynaud D., Barnola J.-M. 2001. Atmospheric CO_2 concentrations over the last glacial termination. *Science* 291: 112-114.

Montenegro A., Brovkin V., Eby M., Archer D., Weaver A.J. 2007. Long term fate of anthropogenic carbon. *Geophys. Res. Lett*. 34: L19707.

Paillard D., Parrenin, F. 2004. The Antarctic ice sheet and the triggering of deglaciations. *Earth Planet. Sci. Lett.* 227: 263-271.

Parrenin F., Paillard, D. 2003. Amplitude and phase of glacial cycles from a conceptual model. *Earth Planet. Sci. Lett.* 214: 243-250.

Pelegrí J.L. 2008. A physiological approach to oceanic processes and glacial-interglacial changes in atmospheric CO_2. *Sci. Mar.* 72: 125-202.

Pepin L., Raynaud D., Barnola J. M., Loutre M.F. 2001. Hemispheric roles of climate forcings during glacial–interglacial transitions as deduced from the Vostok record and LLN-2D model experiments. *J. Geophys. Res*. 106: 31885-31892.

Petit J.R., Jouzel J., Raynaud D., Barkov N.I., Barnola J.-M., Basile I., Bender M., Chappellaz J., Davis M., Delaygue G., Delmotte M., Kotlyakov V.M., Legrand M., Lipenkov V.Y., Lorius C.,

Pépin L., Ritz C., Saltzman E., Stievenard M. 1999. Climate and atmospheric history of the past 420,000 years from the Vostok ice core, Antarctica. *Nature* 399: 429-436.
Schmittner A. 2007. Impact of the Ocean's Overturning Circulation on Atmospheric CO2. In: Ocean Circulation: Mechanisms and Impacts, *Geophysical Monograph Series* 173. American Geophysical Union 10.1029/173GM20
Siddall M., Hönisch B., Waelbroeck C., Huybers P. 2009. Changes in deep Pacific temperature during the mid-Pleistocene transition and Quaternary. *Quat. Sci. Rev.*, doi:10.1016/j.quascirev.2009.05.011
Siegenthaler U., Wenk T. 1984. Rapid atmospheric CO_2 variations and ocean circulation, *Nature* 308: 624-625.
Siegenthaler U. *et al.* 2005. EPICA Dome C carbon dioxide concentrations from 650 to 413 kyr BP. Physikalisches Institut, Universität Bern, doi:10.1594/PANGAEA.472481. In Supplement to: Siegenthaler U., Stocker T. F., Monnin E., Lüthi D., Schwander J., Stauffer B., Raynaud D., Barnola J.-M., Fischer H., Masson-Delmotte V., Jouzel J. 2005. Stable carbon cycle - Climate relationship during the Late Pleistocene. *Science*, 310(5752): 1313-1317.
Sigman D.M., Boyle E.A. 2000. Glacial/interglacial variations in atmospheric carbon dioxide. *Nature* 407: 859-869.
Skinner L.C. 2009. Glacial-interglacial atmospheric CO_2 change: a possible "standing volume" effect on deep-ocean carbon sequestration. *Climate Past* 5: 537-550.
Sloyan B., Rintoul S.R. 2001. The southern limb of the global overturning circulation, *J. Phys. Oceanogr*. 31: 143-173.
Toggweiler J.R., Sarmiento J.L. 1985. Glacial to interglacial changes in atmospheric carbon dioxide: The critical role of ocean surface water at high latitudes. In: Sundquist E., Broecker W.S. (eds.), *The carbon cycle and atmospheric CO_2: Natural variations Archean to present*. Geophysical monograph 32, American Geophysical Union, Washington D.C. pp.163-184.
Toggweiler J.R. 1999. Variation of atmospheric CO_2 by ventilation of the ocean's deepest water. *Paleoceanography* 14: 571-588.
Toggweiler J.R., Russell J.L., Carson S.R. 2006. Midlatitude westerlies, atmospheric CO_2, and climate change during the ice ages. *Paleoceanography* 21: PA2005.
Waelbroeck C., Labeyrie L., Michel E., Duplessy J.C., McManus J.F., Lambeck K., Balbon E., Labracherie M. 2002. Sea-level and deep water temperature changes derived from benthic foraminifera isotopic records. *Quaternary Sci. Rev.* 21: 295-305.
Watson A.J., Naveira Garabato A.C. 2006. The role of southern ocean mixing and upwelling in glacial-interglacial atmospheric CO_2 change, *Tellus* 58B: 73-87.
Wunsch C. 2003. Determining paleoceanographic circulations, with emphasis on the last glacial maximum. *Quaternary Sci. Rev.* 22: 371-385.

Received February 28, 2011. Accepted August 4, 2011.
Published online August 6, 2012.